



Article

Differences in the Corrosive Spalling Behavior of Alumina-Rich Castables: Microstructural and Crystallographic Considerations of Alumina and Calcium Aluminate Matrices

Lise Loison ^{1,*}, Mouna Sassi ², Thorsten Tonnesen ¹, Emmanuel De Bilbao ² , Rainer Telle ¹ and Jacques Poirier ² 

¹ Institute of Mineral Engineering GHI, RWTH Aachen University, 52064 Aachen, Germany; tonnesen@ghi.rwth-aachen.de (T.T.); telle@ghi.rwth-aachen.de (R.T.)

² CNRS, CEMHTI UPR3079, University of Orléans, 45100 Orléans, France; mouna.sassi@cnrs-orleans.fr (M.S.); emmanuel.debilbao@univ-orleans.fr (E.D.B.); jacques.poirier@univ-orleans.fr (J.P.)

* Correspondence: liseloison@yahoo.fr

Received: 24 January 2020; Accepted: 6 May 2020; Published: 11 May 2020



Abstract: The energy transition from the incineration and gasification of fossil fuels to the incineration and gasification of biomass refractory linings is being held up by a severe corrosion issue, caused by high alkali contents and the wide variety of biomass sources. Incinerators optimized for fossil fuels are commonly lined with mullite, Al₂O₃-Cr or SiC-based refractory products; however, those materials are not always suitable for the use of organic fuels. Hibonite (CaO·6Al₂O₃)-based refractory products have shown promising performance because of their high resistance against alkali attacks. Indeed, previous works have shown that the reaction between calcium hexa-aluminate and an alkali does not lead to the strong volume expansion observed with other mineral phases, such as corundum or andalusite. The present work aims to describe the reactions kinetics occurring between hibonite-based raw materials and biomass ashes. Therefore, the three main oxides contained in an average biomass, namely, CaO, SiO₂ and K₂O, were selected to examine the high temperature reactions with a calcium hexa-aluminate matrix. The resulting phase composition and microstructure were compared with the performance of an alumina matrix through, respectively, X-ray diffraction (XRD) analysis and scanning electron microscopy (SEM). The post-mortem observations show a higher extent of reaction for the alumina than for the calcium hexa-aluminate. Moreover, the microstructure of the alumina matrix suffered a strong chemical spalling, while the calcium hexa-aluminate microstructure remained undamaged after the corrosion.

Keywords: refractory; calcium hexa-aluminate; alkali bursting

1. Introduction

The use of biomass fuels challenges the refractory producer in two ways. On the one hand, products used for the incineration and gasification of biomass have to withstand a wide variety of chemical compositions due to the different origins of organic fuels. On the other hand, they also have to be resistant to alkalis, since biomass ashes can contain up to 60 wt.-% of K₂O [1]. Chrome alumina, andalusite and mullite are the oxide products currently used to line biomass incinerators [2]. Unlike alumina, calcium hexa-aluminate has already proven to have high stability when exposed to an alkali, avoiding catastrophic volume expansion known as “alkali bursting.” This property is due to its crystal structure being able to accommodate alkaline atoms. Moreover calcium hexa-aluminate has a similar density to the products formed during the reactions with K₂O or Na₂O; hence, no volume

variation occurs during the reaction. However, the chemical resistance against liquid slag at higher temperatures was hardly tackled [3,4], despite the relevance for incineration and gasification processes, wherein the remaining mineral contents of fuels tend to melt locally and dissolve the refractory components at the lining interface. Beyond the high resistance to alkali bursting, the possible advantages of calcium hexa-aluminate must be defined regarding its stability to molten oxides, in order to consider this refractory phase as an alternative to alumina in refractory products designed for new energy applications. The corrosion behavior of calcium hexa-aluminate and alumina matrix against the main oxides of biomass composition (CaO, SiO₂ and K₂O) must be better understood for the design of incinerators linings. This work emphasizes the microstructural features of two types of matrix, alumina and calcium hexa-aluminate-based ones, and their influences on the corrosion behavior.

2. Materials and Methods

2.1. Refractory Materials

Two types of matrix from refractory castables with comparable microstructures and different mineral compositions were targeted. This allowed us to isolate the effect of calcium hexa-aluminate as a refractory component regarding its potential to replace alpha alumina for specific biomass applications. The alumina and calcium hexa-aluminate matrices were formulated with the same grain size and comparable open porosity, but different chemistry and bonding.

To obtain two different chemistries for the matrix, two different binding systems were used. The binding of the calcium hexa-aluminate matrix was provided by calcium aluminate cement and reactive alumina in order to react with CA₆ during the sintering, and the weight ratios were adjusted to obtain the stoichiometry of the targeted phase. The alumina matrix was bonded with boehmite gel which irreversibly transforms into α -alumina during sintering. The alumina gel was prepared from a commercial boehmite powder (AlO(OH)) containing acetate. After dissolving the powder in 80–85 °C hot water, the dispersion was stabilized through the addition of nitric acid and vaporized to a specific amount. The formulations of the matrices were developed through the optimization of the Andreasen packing coefficient and of the rheological behavior. Then, the proportion of the water was adjusted to obtain the required rheology to cast the samples, but also to obtain comparable open porosity after sintering (Table 1). The raw materials for the castable samples were provided by FIRE C2 partners: the reactive alumina was supplied by Alteo; the tabular alumina and calcium aluminate cement by Imerys; and the calcium hexa-aluminate raw material by Almatix. The dispersant used for the deflocculation was supplied by BASF.

Table 1. Formulations of the matrix samples: (a) gel bonded matrix A; (b) cement-bonded matrix CA₆.

| | | Matrix A | [wt.%] |
|----|--------------------------------|------------------------------|---------------|
| a) | Tabular alumina | 0-0.045 mm | 30.0 |
| | Reactive alumina | PFR | 27.5 |
| | Tabular alumina | 0-0.5 mm | 41.0 |
| | Boehmite gel | | 14.0 |
| | | Matrix CA₆ | [wt.%] |
| b) | Reactive alumina | PFR | 20.0 |
| | Tabular alumina | 0-0.045 mm | 25.0 |
| | Sintered calcium hexaaluminate | 0-0.5 mm | 40.0 |
| | CA cement | Secar71 | 15.0 |
| | Dispersant | FS65 | 0.15 |
| | Water | | 11.0 |

After the casting, the gel bonded matrix was kept under ambient conditions, while the cement-bonded matrix was placed in a climatic chamber for 48 h at 25 °C with a relative moisture content of 95%. Afterwards, both types of samples were kept in a drying chamber at 110 °C for an additional 24 h. The sintering was performed at 1700 °C for 6 h, with an additional dwell time at 500 °C for the cement-bonded matrix to enable the dehydration without damaging the sample due to gas release. The sintering temperature was chosen as a compromise for the calcium hexa-aluminate formation and the obtention of comparable microstructure for both types of matrix. The obtention of a calcium hexa-aluminate matrix was more challenging, because of the difficulty of fully reacting Al_2O_3 and CaO to form CA_6 . The precise adjustment of the chemical composition and the high sintering temperature permit one to obtain a matrix sample containing 99% CA_6 according to XRD measurement and Rietveld quantification.

The characterization of the matrix porous network was based on different standard techniques. The open porosities of the massive matrix samples were measured according to the European standard for refractory samples 993-1. Samples were subsequently grounded down to $<63\mu\text{m}$ to determine pore size with mercury porosimetry using the Autopore IV 9500 Series from Micromeritics and to assess the density of the refractory by means of helium pycnometer using the Ultrapyc 1200e from Quantachrome. The permeability to gas was determined using a permeameter, as described in the standard ISO 8884 with the outlet maintained at atmospheric pressure. While the ISO standard advises expressing the permeability of the refractory material as the average of permeability measurements calculated from three different flow rates, in this work the intrinsic permeability was estimated based on Klinkenberg's model plotting the apparent permeability according to the reciprocal mean pressure to extrapolate the intrinsic permeability value. To address the influence of the porous network of the calcium hexa-aluminate matrix on the dissolution rate, additional samples with enhanced open porosity were produced by adding different amounts of water to the dry composition during the elaboration of the matrix samples.

2.2. Slags

The variety of biomass sources results in a wide range of chemical compositions for the residual ashes. This makes it difficult to address corrosion testing without restricting the conclusions to a few slag compositions. To provide statements extendable to different types of organic fuels residuals, this study was conducted in two steps:

- Quantitative analyses of the reaction extent using a simplified slag composition narrowed down to the three main components, SiO_2 , CaO and K_2O —based on chemical compositions reviewed in [1].
- Visual observations of the spalling comparing the effect of synthetic slag composition with natural wood ash (Figure 1) to validate the correlation.

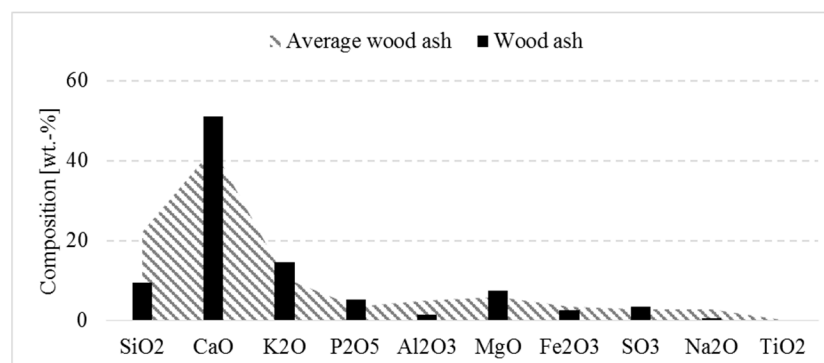


Figure 1. Average composition of wood ash from [1] compared with the chemical composition of the wood ash used in the present study.

To isolate the influences of the main oxides contained in biomass ashes, SiO_2 , CaCO_3 and K_2CO_3 powders were mixed (all reagent grade) to obtain SiO_2 - CaO - K_2O in weight ratio 2:2:1. The ternary slag CSK was decarbonated at 1000 °C for 12 h and melted at 1400 °C/1 h for a final homogenization prior to quenching in water and grinding.

2.3. Corrosion Testing

To examine the matrix reactions, 0.9 g of the synthetic slag was mixed with a few drops of ethanol for uniaxial pressing to parallelepipedic dimensions (5 × 5 × 25 mm) to be deposited on a slice of refractory matrix (5 × 10 × 30 mm). The corrosion couple was introduced in a resistive furnace at 1400 °C for different time periods and quenched in water prior to X-ray diffraction analysis.

In this corrosion test, the quantity of slag is low and might limit the reaction once the slag is saturated with the refractory. Moreover the testing is static, i.e., absent movement of fluid, avoiding erosion effects and lowering the transport rates. The temperature distribution is considered homogeneous across the sample volume and the matrix samples are not pre-heated. It can be considered that they undergo a severe thermal shock as they are introduced in the furnace at 1400 °C. However, the influence of this microstructural damage is assumed to be negligible on the resulting phase composition.

For the comparison with the wood ash, cylindrical samples of matrix (H10 mm × D50 mm) are covered with a pressed tabled of 5 g of ash. The samples are heated in a resistive furnace with 2 K/min and kept 2 h and 24 h at 1550 °C before cooling naturally down to room temperature.

The testing temperatures were adapted to the melting temperatures of the synthetic and biomass slag, respectively 1224 °C and 1430 °C, measured with hot stage microscopy according to the European standard 51730.

2.4. X-ray Diffraction

Two types of X-ray diffraction (XRD) analysis were conducted:

- Space-resolved XRD to consider the influence of the microstructure on the reaction depth.
- Quantitative XRD to evaluate the extent of reaction.

Space-resolved XRD was performed after sectioning the corroded samples perpendicularly to the refractory/slag interface. The sample was placed on the XYZ stage of the diffractometer. A collimator was mounted on the incident X-ray beam using a snout of 1 mm diameter, and three XRD measurements were performed at a given distance from the interface before adding the recorded signals to obtain a diffractogram corresponding to a surface of 2.4 mm². The scan was performed from 5° to 90° [2θ] with step of 0.02° and 384 s/step. The XRD patterns were recorded on a Bruker D8 automated diffractometer using Ni-filtered Cu-Kα1 radiation ($\lambda = 1.5406 \text{ \AA}$).

The influence of matrix porosity on reaction extent of CA_6 samples was evaluated using quantitative XRD. After reacting with 0.9 g of synthetic slag for different durations, the samples were ground <63 microns with vibrating disc mill. The XRD patterns were collected in the Bragg–Brentano (θ -2 θ) geometry between 5° and 90° (2 θ) in 0.01° steps at 96 s.step⁻¹ and $\lambda = 1.5406 \text{ \AA}$.

Based on the recorded XRD patterns, a quantification by Rietveld refinement with the software TOPAS from Bruker using the fundamental parameters was performed to determine the amounts of the coexisting phases. The preferred orientation of calcium hexa-aluminate was considered in the structure card of CA_6

It is assumed that the amorphous content (X_a) of the ex situ sample should relate to the amount of high temperature liquid phase due to the rapid cooling. The direct method of degree of crystallinity (DOC) is used to quantify the liquid phase that forms in the reaction with the synthetic slag. This method calculates the amorphous phase amount by relating the area under the crystalline peaks to the area under the amorphous bump (Equations (1) and (2)):

$$\text{DOC} = (\text{Crystalline area})/(\text{Crystalline area} + \text{Amorphous area}) \quad (1)$$

$$X_a = 1 - \text{DOC} \quad (2)$$

To further reduce the uncertainty of the amorphous quantification, the liquid amount yield by the reaction is determined by subtracting the amorphous content calculated for the uncorroded sample.

$$\text{Liq} = \Delta(X_a) = X_a (\text{Corroded}) - X_a (\text{Uncorroded}) \quad (3)$$

This method was used to quantify the liquid formed in matrix samples of CA_6 with different open porosities after 2 h and after 24 h. Both Rietveld and DOC quantifications enable the calculation of the CA_6 content remaining in the matrix sample. The decrease of the CA_6 content was used to estimate the dissolution progress. The extent of dissolution was calculated based on the decrease of CA_6 content according to reaction duration. The values are expressed in an arbitrary unit of calcium hexa-aluminate loss per hour (%/h), while considering that the samples all have the same contact area as the slag; namely, $5 \times 25 \text{ mm}^2$.

3. Results

3.1. Characterization of the Porosity

For the resistance against slag infiltration, some microstructural properties of the matrix are relevant, such as the open porosity, the pore sizes and the permeability to gas. The rheology of matrix CA_6 requires lower amounts of water during the mixing of the raw materials. However, the resulting open porosity is slightly higher than for matrix A. This might be due to the poorer tendency for densification of calcium hexa-aluminate reported in the literature, leading to higher open porosity compared to alumina [5]. Although comparable amounts of open porosity were achieved for both matrices, the porous network seems to exhibit different features. The use of a colloidal binder led to a greater average pore diameter of $3.0 \mu\text{m}$, while the deflocculated cement binding resulted in a lower average pore diameter of $1.0 \mu\text{m}$ (Figure 2).

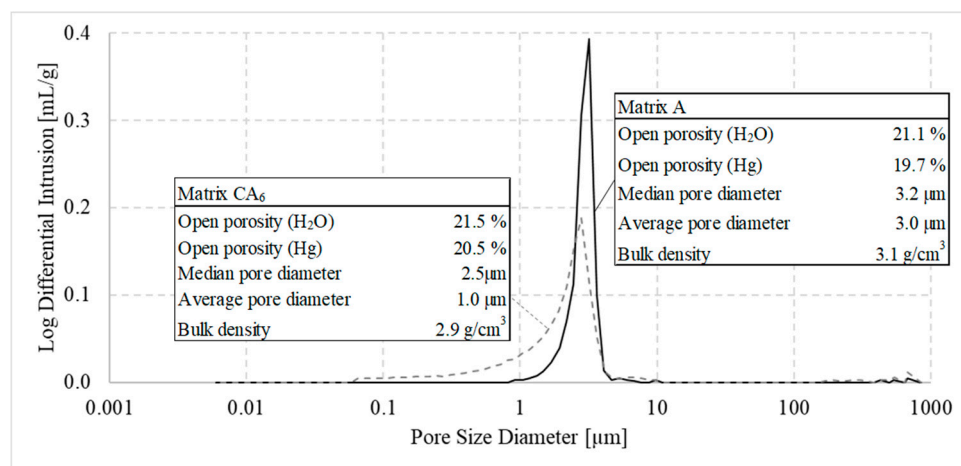


Figure 2. Pore size distribution after sintering at $1700 \text{ }^\circ\text{C}/6 \text{ h}$.

The permeability to liquid was determined by a multi-point measurement of gas permeability to determine the intrinsic permeability. The exploitation of the results is based on Dranchuk interpretation reported in [6] and its application to refractory products is described in [7,8].

The alumina matrix exhibits a permeable microstructure with an intrinsic permeability of 22.7 mD against 4.9 mD for the calcium hexa-aluminate matrix (Figure 3). The permeability value represents the interconnected open porosity and is a relevant parameter for the resistance to infiltration.

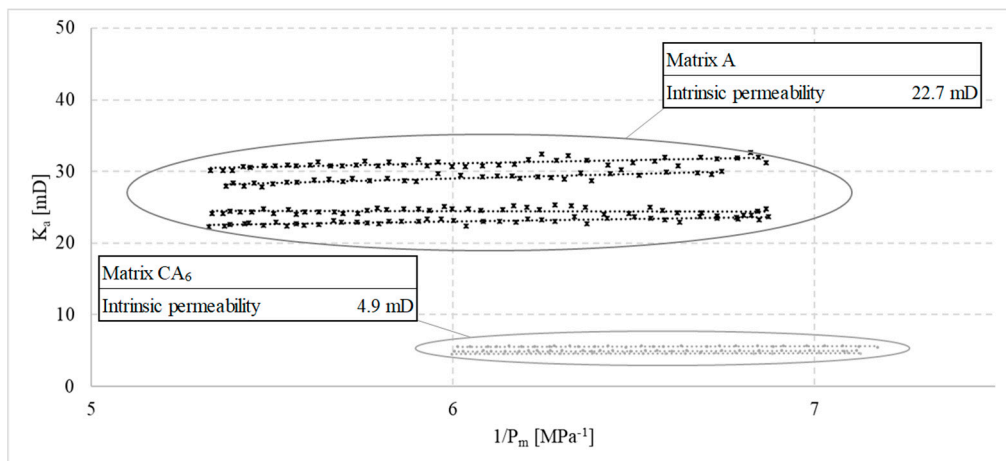


Figure 3. Permeability of alumina and calcium hexa-aluminate matrix.

3.2. Resistance to Structural Spalling

After reacting at 1400 °C with CSK slag for 24 h, the matrix samples revealed strong differences in their geometries (Figures 4 and 5). The samples were kept massive for space-resolved XRD using an XYZ table as the sample holder.

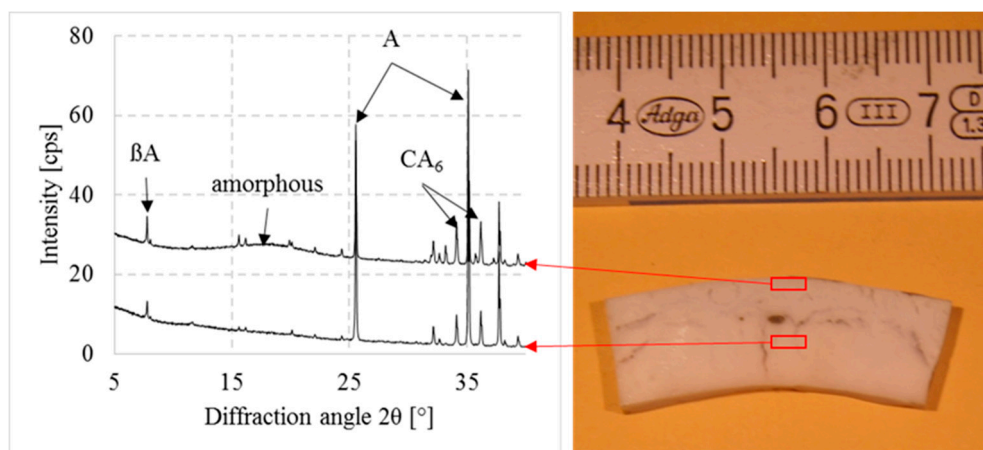


Figure 4. Space-resolved XRD of matrix A after 24 h in contact with CSK slag at 1400 °C and quenching in water.

At the surface of the alumina matrix, which was covered with slag, alumina (A) was present with high amounts of calcium hexa-aluminate (CA_6), potassium β -alumina (βA) and amorphous phase. The measurement performed at 5 mm from the interface shows an attenuated presence of the reaction products. The gradient in the mineralogical composition between the interface and the core of the sample is strongly marked. The difference of volume between the reaction products and the alumina leads to the curved shape of the sample after cooling and the cracking observed in Figure 4.

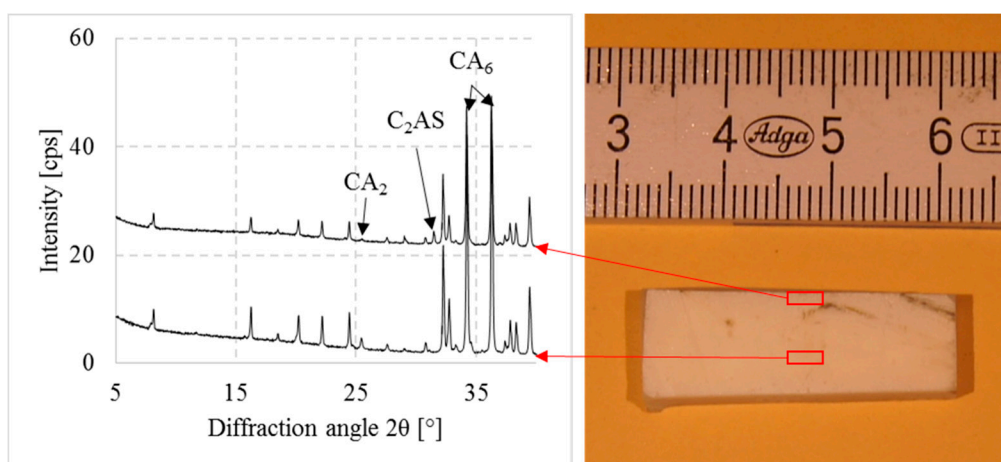


Figure 5. Space-resolved XRD of matrix CA6 after 24 h in contact with CSK slag at 1400 °C and quenching in water.

While the alumina sample shows a strong deformation after corrosion (Figure 4), the calcium hexa-aluminate matrix remains dimensionally stable (Figure 5). The XRD measurements show the main phase to be calcium hexa-aluminate, and traces of Gehlenite (C_2AS) and Grossite (CA_2) show the low reactivity of the calcium hexa-aluminate matrix. The silica-containing phase was only present at the interface. Since the extent of reaction at the interface is low, only a slight difference was observed in the XRD measurements of the surface and of the core of the sample. At a distance of 5 mm from the interface, calcium hexa-aluminate was present with traces of calcium di-aluminate. The density variations were measured on the ground samples with helium pycnometer (Table 2).

Table 2. Density measurements of the matrix samples.

| [g/cm ³] | Before Corrosion with CSK 1400 °C/24h | After Corrosion with CSK 1400 °C/24h |
|------------------------|---------------------------------------|--------------------------------------|
| Matrix A | 4.0 | 3.4 |
| Matrix CA ₆ | 3.7 | 3.4 |

The starting density for matrix A was higher, with a value of 4.0 g·cm⁻³, than for matrix CA₆, with a value of 3.7 g·cm⁻³, in agreement with the theoretical densities. After corrosion, both matrix samples exhibited the same density of 3.4 g·cm⁻³. The density measured after corrosion is the sum of all the single contributions of the different phases coexisting in the sample. The reaction with CSK slag generates low density products, which require a greater volume than the original phase. The density gradient was lower in the case of the matrix CA₆, and the reaction products could expand in the open porosity without macroscopic volume expansion.

The observations after corrosion with the model slag are compared with the resulting sample geometry after corrosion with wood ash (Figure 6)

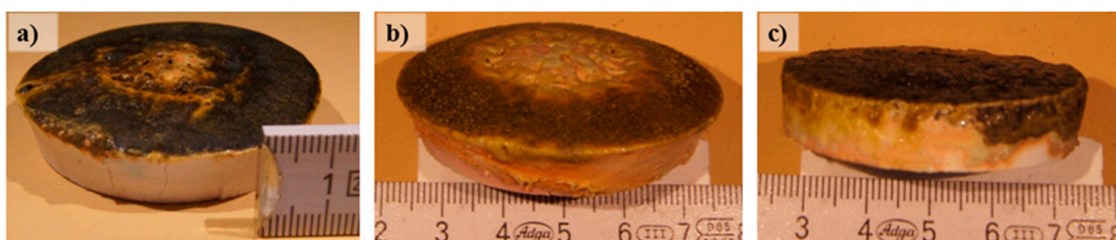


Figure 6. Matrix samples after corrosion with wood ash at 1550 °C: (a) matrix A after 2 h; (b) matrix A after 24 h; (c) matrix CA₆ after 24 h

In the case of the alumina matrix, a strong structural spalling is visible after corrosion with wood ash, while calcium hexa-aluminate seems to react without volume variations, and hence, without damaging the initial microstructure of the refractory product.

The volume variations are calculated based on geometry measurements after the natural cooling of the corroded samples (Figure 7).

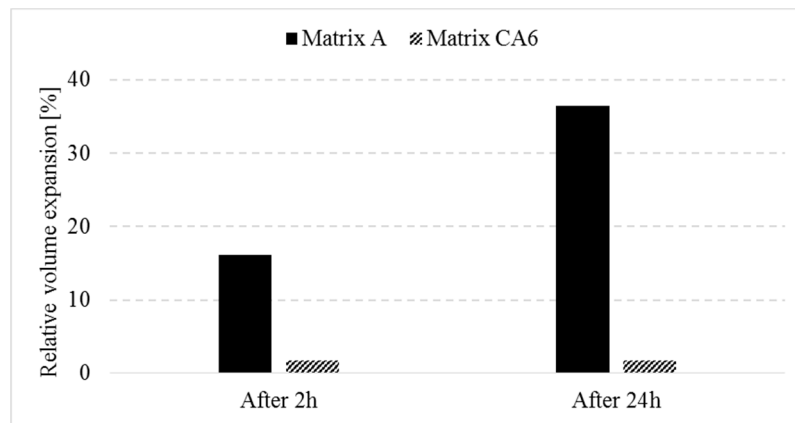


Figure 7. Post-mortem volume expansion after corrosion with wood ash at 1550 °C.

After corrosion with wood ash, the calcium hexa-aluminate sample showed a low expansion of 2 Vol.-% which remained constant after different testing durations. On the contrary, the alumina matrix exhibited a strong volume expansion of 16 Vol.-% after 2 h at 1550 °C, which increased up to 36 Vol.-% after 24 h.

3.3. Influence of the Porosity

In order to test the influence of the matrix's porosity on the corrosion behavior, different matrixes were cast with different amounts of water. The open porosity was measured with water according to the European standard 993-1 and with mercury porosimetry (Figure 8).

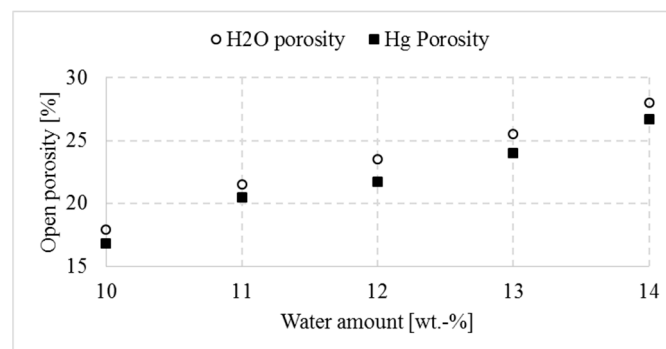


Figure 8. Open porosity of matrix CA₆ after sintering at 1700 °C/6 h according to the amount of water added for casting.

The open porosity measured with water yielded slightly higher porosity values than mercury porosimetry. Since the mercury measurements were carried out on ground samples with a more intrusive fluid, only micropores were reached, unlike water measurements comprising both micro- and macroporosity. The dense refractory matrices were mainly composed of microporosity, explaining why the differences between both methods were low. The open porosity increased linearly with the amount of water added during the mixing of the matrix components. No significant variations of the pore diameter were measured with the mercury porosimetry, and the values are shown in Table 3.

Table 3. Average pore diameter of matrix CA₆ after sintering at 1700 °C/6 h measured with mercury porosimetry.

| Water Amount | [wt.%] | 10 | 11 | 12 | 13 | 14 |
|-----------------------|--------|-----|-----|-----|-----|-----|
| Median pore diameter | [μm] | 1.9 | 2.5 | 2.5 | 2.6 | 3.7 |
| Average pore diameter | [μm] | 0.6 | 1.0 | 1.3 | 1.3 | 1.8 |

The different samples were corroded with 0.9 g of slag CSK to determine the rate of dissolution of calcium hexa-aluminate after 2 h and after 24 h. The values are compared in Figure 9, expressed in an arbitrary unit of calcium hexa-aluminate loss per hour (%/h), while considering the samples all had the same contact area with the slag; namely, 5 × 25 mm².

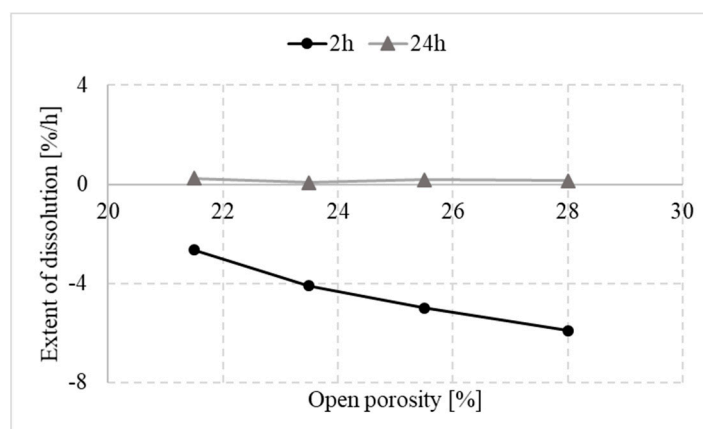


Figure 9. Rate of dissolution of matrix CA₆ in CSK slag at 1400 °C according to the open porosity expressed as the decrease in CA₆ content of the sample per hour.

After 2 h in contact with CSK slag, the rate of dissolution was strongly influenced by the open porosity of the matrix. The original matrix CA₆ compared previously with the alumina matrix exhibited an open porosity of 21.5%, and the dissolution rate after 2 h was −2.7%/h. The matrix with 28% open porosity, showed after 2 h a dissolution rate of −5.9%/h, with a linear increase of the dissolution rate according to the open porosity. After 24 h, the further dissolution rate was close to zero, and the open porosity did not have any influence anymore. The open porosity influences the rate of dissolution at the beginning of the corrosion process, with lower dissolution rates for lower open porosity. As the reaction advanced, the dissolution slowed down strongly due to the saturation of the liquid phase declining the impact of the open porosity. That is consistent with the literature, confirming that the rate of dissolution increases linearly with the percentage of apparent porosity [9].

3.4. Morphology of Calcium Hexa-Aluminate

As mentioned in the introduction, the calcium hexa-aluminate phase can exhibit different types of morphology. The Rietveld refinement can also determine qualitatively the shape of the calcium hexa-aluminate crystallites. A tool is proposed in the TOPAS interface to assess the preferred orientation of one phase in the quantification of the crystalline compounds. The quantification can indeed be distorted if the texture is not considered for the refinement [10]. A coefficient is then attributed to the (0 0 1) direction planes, indicating the degree of texture. A coefficient close to one refers to randomly-oriented crystallites, while a coefficient smaller than one indicates the preferred orientation of plate crystallites (Figure 10).

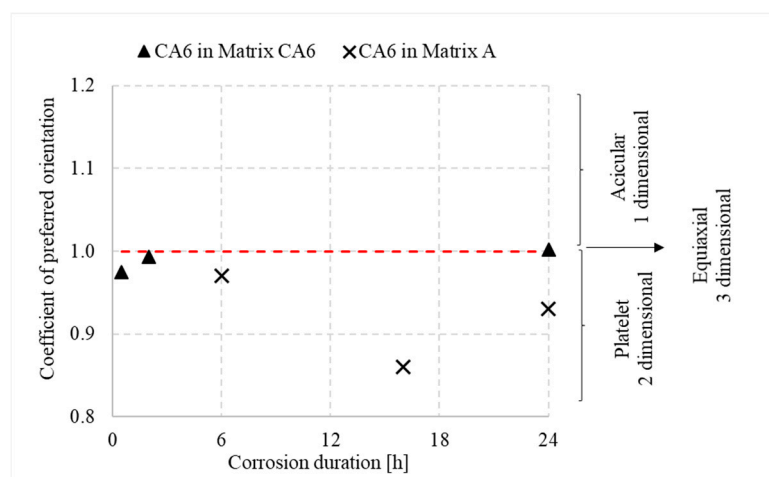


Figure 10. Coefficient of preferred orientation for the calcium hexa-aluminate phase obtained from the Rietveld refinement performed after corrosion with CSK slag at 1400 °C.

The coefficient indicates two types of orientation for the calcium hexa-aluminate phase, according to the two types of growth:

The sintered calcium hexa-aluminate obtained either as sintered aggregate or from the sintering between calcium aluminate cement and reactive alumina. Those calcium hexa-aluminate crystals present in the matrix CA₆ were randomly oriented with a coefficient close to one (Figure 10).

The precipitated calcium hexa-aluminate obtained from the dissolution of alumina matrix in the slag CSK. Those crystals were textured, and the coefficient lower than one indicates an oriented platelet morphology (Figure 10). The platelet morphology was observed on the crystals grown in the intergranular melt examined with SEM as well (Figure 11).

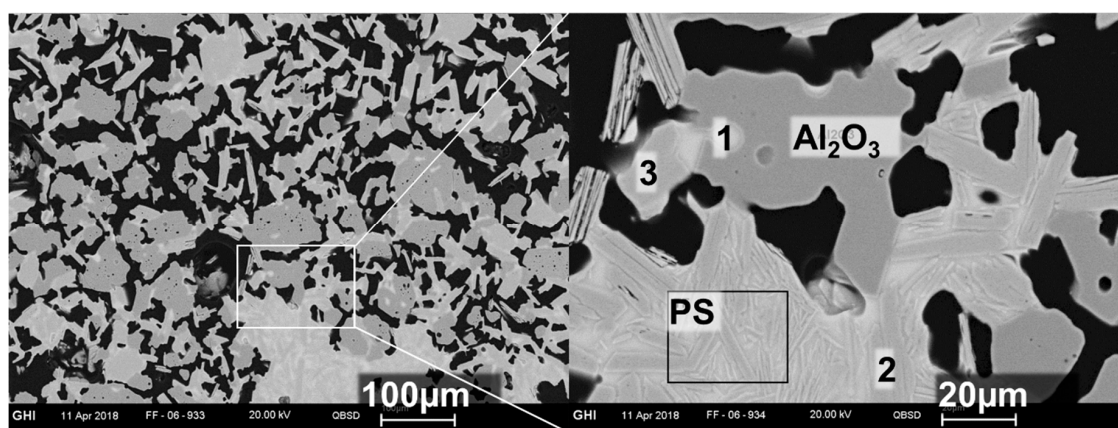


Figure 11. Micrographs of calcium hexa-aluminate formed in matrix A after corrosion with CSK slag at 1400 °C/150 h and quenching in water.

The morphology of the calcium hexa-aluminate as a reaction product is visible in Figure 11. The platelets precipitate from an intergranular liquid phase in the vicinity of the tabular alumina being dissolved. The EDX #3 reveals a chemical composition close to the stoichiometry of calcium hexa-aluminate, while the EDX #1 and #2 comprise calcium hexa-aluminate and the liquid phase composed of the slag elements, depleted in potassium and enriched in alumina and sodium (Table 4).

Table 4. EDX measurements from Figure 11.

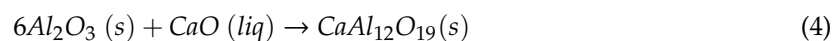
| [wt. %] | Na ₂ O | Al ₂ O ₃ | SiO ₂ | K ₂ O | CaO |
|-----------------|-------------------|--------------------------------|------------------|------------------|------|
| Partial surface | 0.5 | 75.2 | 11.3 | 0.9 | 12.2 |
| 1 | 1.9 | 38.3 | 34.7 | 3.5 | 21.7 |
| 2 | 1.6 | 54.5 | 24.3 | 2.5 | 17.2 |
| 3 | - | 91.4 | - | - | 8.6 |

4. Discussion

Different amounts of water were added during the mixing to the dry composition of the calcium hexa-aluminate matrix in order to determine the influence of the capillary network on the corrosion. The resulting open porosity after sintering of the matrix is correlated to the additional amount of water (Figure 8). After testing the corrosion with CSK slag, it was observed that the enhanced open porosity increased, linearly, the rate of dissolution (Figure 9). The objective of this trial was to determine the contribution of the matrix's microstructure to the dissolution rate values, to assess whether the better performance of matrix CA₆ could be attributed to the lower permeability and smaller pore sizes of the microstructure. However, the addition of water to increase the open porosity does not lead to any significant increase of the pore size (Table 3). The comparison with the microstructure of matrix A was not achieved, and the influences of the microstructural features on the high corrosion resistance of matrix CA₆ remains+ undefined.

Two types of morphologies could be observed for the calcium hexa-aluminate phase. The sintered calcium hexa-aluminate exhibits a random orientation in its crystalline structure, while the precipitated calcium hexa-aluminate is textured and exhibits a platelet morphology (Figure 10). The equiaxed grains observed in matrix CA₆ after sintering are not representative of the morphology usually obtained in a calcium aluminate cement-bonded castable. According to literature [11], this could be attributed to the enhanced sintering temperature of 1700 °C, leading to the growth of platelets into equiaxed grains.

The plate-like morphology was observed in the alumina matrix, after undergoing a strong volume expansion. The structural spalling was not attributed to the alkali reaction from the potassium contained in the slag, but rather to the reaction with the calcium (Figure 4). The expansive formation of calcium hexa-aluminate was due to the lower density of the phase formed. The volume increase from corundum to calcium hexa-aluminate can be calculated as follows:



$$\Delta V = \frac{V_{CaAl_{12}O_{19}} - 6V_{Al_2O_3}}{6V_{Al_2O_3}} = +14.7\% \quad (5)$$

Considering for alumina 102g/mol, 3.99g/cm³ and for calcium hexa aluminate 668g/mol, 3.79 g/cm³

Though the theoretical volume increase is lower than the one caused by alkali reaction (+26.5% from [12]), the volume expansion for the transformation of alpha alumina into calcium hexa-aluminate is considerable. Since calcium hexa-aluminate exhibits a low density and a low reactivity, no structural spalling was observed after corrosion in matrix CA₆, either with the model slag, or with the wood ash.

5. Conclusions

The advantages of hexa-aluminate, compared to alumina as a matrix of castables, for the applications of biomass incineration or gasification, have been enriched in this paper. While the chemical stability of calcium hexa-aluminate is attested to, both against dissolution with lime silicate slags and against alkali-bursting [12], this work has shown that the advantages of this refractory mineral can be microstructural as well. The comparison of a calcium hexa-aluminate matrix provided

by calcium aluminate cement and reactive alumina and an alumina matrix bonded with boehmite sol-gel show that the calcium hexa-aluminate matrix presents:

- A lower permeability and a lower average pore diameter.
- A better resistance to structural spalling induced by calcium aluminate precipitation.
- A lower reactivity in contact with biomass ashes.

Thus, hibonite ($\text{CaO}\cdot 6\text{Al}_2\text{O}_3$)-based refractory castables show promising performances for the incineration and gasification of biomasses.

Author Contributions: Methodology, L.L., M.S., T.T., E.D.B., R.T., J.P., Data curation, L.L., M.S., T.T., E.D.B., R.T., J.P., original draft preparation, L.L., writing—review and editing, L.L., supervision, T.T., E.D.B., R.T., J.P. All authors have read and agreed to the published version of the manuscript.

Funding: This research was funded by FIRE (Federation for International Research for Refractory Education).

Conflicts of Interest: The authors declare no conflict of interest

References

1. Vassilev, S.V.; Baxter, D.; Andersen, L.K.; Vassileva, C.G. An overview of the chemical composition of biomass. *Fuel* **2010**, *89*, 913–933. [[CrossRef](#)]
2. Bennett, J.P.; Kwong, K.-S.; Powell, C.A. *Issues Impacting Refractory Service Life in Biomass/Waste Gasification*; International Corrosion Conference Series; NETL: Pittsburgh, PA, USA; Morgantown, WV, USA; Albany, OR, USA, 2007.
3. Vazquez, B.A.; Pena, P.; de Aza, A.H.; Sainz, M.A.; Caballero, A. Corrosion mechanism of polycrystalline corundum and calcium hexaaluminate by calcium silicate slags. *J. Eur. Ceram. Soc.* **2009**, *29*, 1347–1360. [[CrossRef](#)]
4. Gentile, A.L.; Foster, W.R. Calcium hexaaluminate and its stability relations in the system $\text{CaO}\text{-Al}_2\text{O}_3\text{-SiO}_2$. *J. Am. Ceram. Soc.* **1963**, *46*, 74–76. [[CrossRef](#)]
5. Criado, E.; Pena, P.; Caballero, A. Influence of processing method on microstructural and mechanical properties of calcium hexaaluminate compacts. *J. Ceram. Sci.* **1988**, *14*, 193–198.
6. Dranchuk, P.M.; Kolada, L.J. Interpretation of Steady Linear Visco-Inertial Gas Flow Data. *J. Can. Pet. Technol.* **1968**, *7*, 36–40. [[CrossRef](#)]
7. De Bilbao, E.; Loison, L.; Hbiriq, Y.; Orgeur, C.; Brassamin, S.; Tonnesen, T.; Poirier, J. Intrinsic permeability of refractories from gas permeability measurements: Comparison of results. *Ceram. Int.* **2018**, *44*, 2900–2910. [[CrossRef](#)]
8. Loison, L.; de Bilbao, E.; Tonnesen, T.; Telle, R. Determination of permeability for refractories: From standard test methods to improved interpretation technique of the experimental data. *Refract. Worldforum* **2017**, *9*, 113–116.
9. Schacht, C.A. Corrosion of refractories. In *Refractory Handbook*; Marcel Dekker Inc.: New York, NY, USA, 2004; pp. 39–77.
10. Dickson, M.J. The significance of texture parameters in phase analysis by X-ray Diffraction. *J. Appl. Crystallogr.* **1969**, *2*, 176–180. [[CrossRef](#)]
11. Dominguez, C.; Chevalier, J.; Torrecillas, R.; Gremillard, L.; Fantozzi, G. Thermochemical properties and fracture mechanisms of calcium hexaaluminate. *J. Eur. Ceram. Soc.* **2001**, *21*, 907–917. [[CrossRef](#)]
12. Büchel, G.; Buhr, A.; Gierisch, D.; Racher, R.P. Alkali- and CO-resistance of dense calcium hexaaluminate Bonite. In Proceedings of the 48th International Colloquium on Refractories, Aachen, Germany, 28–29 September 2005; pp. 208–214.



© 2020 by the authors. Licensee MDPI, Basel, Switzerland. This article is an open access article distributed under the terms and conditions of the Creative Commons Attribution (CC BY) license (<http://creativecommons.org/licenses/by/4.0/>).